NIPPON STEEL TECHNICAL REPORT No. 124 SEPTEMBER 2020

Technical Report

UDC 621. 746 . 27 : 621 . 746 . 395 . 4

Numerical Analysis Study for Clogging Behavior of Immersion Nozzle

Nobuhiro OKADA* Hitoshi FUNAGANE
Takehiko TOH

Abstract

In the continuous casting of aluminum-killed steel, alumina adheres to the immersion nozzle, causing the molten steel flow path to close and adversely affect the flow in the mold. The adhesion of inclusions to refractories has been studied for the reaction mechanism between the refractories and the molten steel. In this study, we investigated the adhesion due to molten steel flow using a numerical analysis model. In order for micro-inclusions to adhere to the wall surface in the turbulent flow in the immersion nozzle, it is essential to pass into the viscous bottom layer by turbulent diffusion, so numerical analysis was conducted using a model based on the turbulent diffusion. As a result, near the sliding gate, nozzle clogging is represented by the velocity-dependent model, but the clogging of the outlet port could not be represented. The Linder model and the Oeters model could be represented by the clogging of the outlet port.

1. Introduction

In the continuous casting of steel, molten steel is poured from a tundish through an immersion nozzle into a mold. The molten steel flow in the mold has a large effect on the quality of cast slabs. It is desirable that the flow of the molten steel through the immersion nozzle should be stable. When aluminum-killed steel is continuously cast, however, alumina and other nonmetallic inclusions (hereinafter simply referred to as inclusions) adhere to the inside of the immersion nozzle, clog the molten steel flow path, adversely affect the molten steel flow in the mold, and eventually cause deterioration of the slab quality.

Many studies have been conducted on this clogging mechanism of the immersion nozzle. Early studies investigated immersion nozzles used for continuous casting, evaluated the refractories and adhered materials of the immersion nozzles, and reported the results.[1–3] Sasai et al.[4] performed basic experiments to clarify the reaction mechanism between silica-containing alumina graphite, an immersion nozzle material, and molten steel, and reported the reaction mechanism involved.

Also, the adhesion of inclusions to the immersion nozzle is considered to affect the molten steel flow near the nozzle refractory. Singh[5] reported the mechanism whereby inclusions suspended in the molten steel adhere to and deposit on the nozzle refractory wall. Singh's mode considers wettability and surface tension action but not the inclusion motion process near the nozzle refractory wall. Taniguchi and Kikuchi[6] conducted a model experiment and reported a mechanism whereby the lift force produced by the velocity gradient near the nozzle refractory wall acts on the motion of inclusions. The model of Taniguchi and Kikuchi evaluated the adhesion speed of inclusions to the nozzle refractory wall according to the theories of Rubinow and Kellyer[7] and Saffman,[8] but could not explain the adhesion phenomenon of inclusions because of the tendency for the inclusions in the downward flow to move away from the nozzle refractory wall. Since it is difficult for this model to explain the process in which minute inclusion particles, a few micrometers in size, reach and adhere to the nozzle refractory wall in the molten steel flow field in the immersion nozzle, Mukai et al.[9] proposed an inclusion adhesion model by focusing on the motion of inclusions by turbulent diffusion. Linder[10] and Oeters[11] reported models that consider that turbulent diffusion controls the adhesion of inclusion particles to the nozzle refractory wall.

As reviewed by Thomas and Zhang,[12] numerical analysis models of continuous casting in recent years have become able to make relatively detailed calculations, including the tundish and the im-

* Senior Researcher, Dr.Eng., Mathematical Science & Technology Research Lab., Advanced Technology Research Laboratories
20-1 Shintomi, Futtsu City, Chiba Pref. 293-8511

mersion nozzle. The molten steel flow in the immersion nozzle is affected by argon gas and sliding gates and produces a complicated flow field accompanying gas entrapment as reported by Kato et al.[13] However, it is still difficult to accurately consider flow control devices like sliding gates and stoppers and to perform detailed fluid analysis by considering gas-liquid two-phase flow due to argon gas injection. For example, Guitierrez et al.[14] conducted the fluid analysis of molten steel through the immersion nozzle by a model that considers the Saffman lift force and studied the velocity of inclusions adhering to the upper part of the nozzle, but they did not consider sliding gates and argon gas.

As described above, it is still impossible to numerically analyze accurately the flow of bubbles and molten steel in the immersion nozzle. In this study, we investigated nozzle clogging by numerical analysis with a model that ignored argon gas and considered the shape of sliding gates and outlet ports.

2. Mathematical Model

2.1 Fluid analysis model

Fluid analysis calculations were performed by using the commercial fluid analysis software ANSYS Fluent®. Governing equations of fluid analysis are given by Equations (1) to (3). Equation (1) is the law of mass conservation and Equation (2) is a momentum transport equation. The second term on the left-hand side of Equation (2) is a momentum convection term. The first-order upwind scheme was used to calculate the momentum convection term. The second term on the right-hand side of Equation (2) is a viscosity term. The components of the viscosity term are as shown by Equation (3).

$$\frac{\partial \rho}{\partial t} + \nabla\cdot(\rho\vec{v}) = 0 \tag{1}$$

$$\frac{\partial}{\partial t}(\rho\vec{v}) + \nabla\cdot(\rho\vec{v}\vec{v}) = -\nabla p + \nabla\cdot\bar{\bar{\tau}} + \rho\vec{g} \tag{2}$$

$$\bar{\bar{\tau}} = \mu\left(\nabla\vec{v} + \nabla\vec{v}^{\mathrm{T}} - \frac{2}{3}\nabla\cdot\vec{v}I\right) \tag{3}$$

where ρ is specific gravity, $\vec{v}$ is the flow velocity vector, p is pressure, $\vec{g}$ is the gravitational acceleration vector, μ is viscosity, I is the unit matrix, and T is the transpose matrix.

The molten steel flow in the immersion nozzle is turbulent. The standard k-ε model was used as the turbulence model. Here, k and ε are turbulent energy and turbulent energy dissipation rate and are calculated as shown by Equations (4) and (5), respectively.

$$\rho\frac{\partial}{\partial t}(k) + \nabla\cdot(\rho\vec{v}k) = \nabla\cdot\left[\left(\mu + \frac{\mu_t}{\sigma_k}\right)\nabla k\right] + G_k - \rho\varepsilon \tag{4}$$

$$\rho\frac{\partial}{\partial t}(\varepsilon) + \nabla\cdot(\rho\vec{v}\varepsilon) = \nabla\cdot\left[\left(\mu + \frac{\mu_t}{\sigma_\varepsilon}\right)\nabla\varepsilon\right] + C_{1\varepsilon}G_k - C_{2\varepsilon}\rho\frac{\varepsilon^2}{k} \tag{5}$$

where μ_t is turbulent viscosity and calculated by

$$\mu_t = \rho C_\mu \frac{k^2}{\varepsilon} \tag{6}$$

G_k is the turbulent energy generation rate. The coefficients of the standard model are $C_{1\varepsilon}=1.44$, $C_{2\varepsilon}=1.92$, $\sigma_\varepsilon=1.3$, $\sigma_k=1.0$, and $C_\mu=0.09$.

Let N be the inclusion concentration and $\vec{u_P}$ be the inclusion motion velocity. A user subroutine was developed from the transport equation expressed by Equation (7) and used to calculate the transport equation. V_T is the adhesion velocity of inclusions to the nozzle refractory wall and described in the next section.

$$\frac{\partial}{\partial t}(N) + \nabla\cdot(\vec{u_P}N) = -V_T \tag{7}$$

The inclusions in the molten steel are assumed to be rigid particles and their motion velocity $\vec{u_P}$ is calculated by Equation (8).

$$\frac{d\vec{u_P}}{dt} = \frac{\vec{v}-\vec{u_P}}{\tau_r} + \frac{\vec{g}(\rho_P-\rho)}{\rho_P} \tag{8}$$

where ρ_P and τ_r are the specific gravity of particles and relaxation time, respectively, and are given by

$$\tau_r = \frac{\rho_P d_P^2}{18\mu} + \frac{24}{C_d \mathrm{Re}} \tag{9}$$

where d_P and Re are the particle diameter and particle Reynolds number, respectively, and are given by Equation (10). C_d is the resistance coefficient of particles and depends on Re.

$$\mathrm{Re} = \frac{\rho d_P|\vec{u_P}-\vec{v}|}{\mu} \tag{10}$$

When the particle motion velocity expressed by Equation (8) reaches the steady state, it is called the terminal velocity. Depending on Re, this velocity may be considered in the following three cases as expressed by Equations (11) to (13).[15]

Stokes' law (Re<2) $$u_P = \frac{g(\rho_P-\rho)d_P^2}{18\mu} \tag{11}$$

Allen's law (2<Re<500) $$u_P = \left(\frac{4g^2(\rho_P-\rho)^2}{225\mu\rho}\right)^{1/3} d_P \tag{12}$$

Newton's law (Re<500) $$u_P = \left(\frac{4g(\rho_P-\rho)}{3\times0.44\rho}d_P\right)^{1/2} \tag{13}$$

The Saffman lift force F_s is expressed by Equation (14) and the terminal velocity that accounts for the Saffman lift force is given by Equation (15).[6, 8]

$$F_s = 1.62\sqrt{\rho\mu}\,u_P\sqrt{\left|\frac{\partial v}{\partial n}\right|}\,d_P^2 \tag{14}$$

$$u_P = \frac{1.62\mu\sqrt{\rho\left|\frac{\partial v}{\partial n}\right|}d_P}{3\pi\sqrt{\mu}} \tag{15}$$

When calculated by Equation (9), the relaxation time of inclusion particles in the molten steel is short. The inclusion particles reach the terminal velocity relatively quickly. To reduce the calculation time, the motion velocity of inclusion particles was calculated by assuming that it was the sum of the molten steel flow velocity plus the above-mentioned terminal velocity.

Figure 1 schematically illustrates the inclusion adhesion distribution of the immersion nozzle. The adhesion of inclusions by the molten steel flow is considered to occur where the main stream of the molten steel separates from the nozzle refractory wall.[16, 17] This study performed calculations on the regions near the sliding gate and the outlet ports where the molten steel flow is likely to separate from the nozzle refractory wall.

Figure 2 shows the calculation geometry and the calculation mesh used for the numerical analysis. The inside diameter of the im-

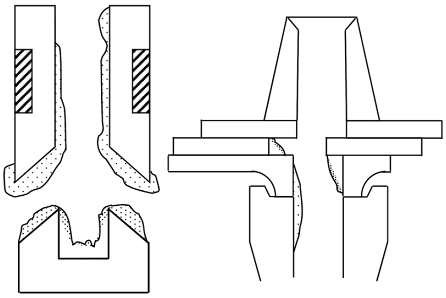

(a) Outlet port (b) Sliding gate

Fig. 1 Schematic image of nozzle clogging

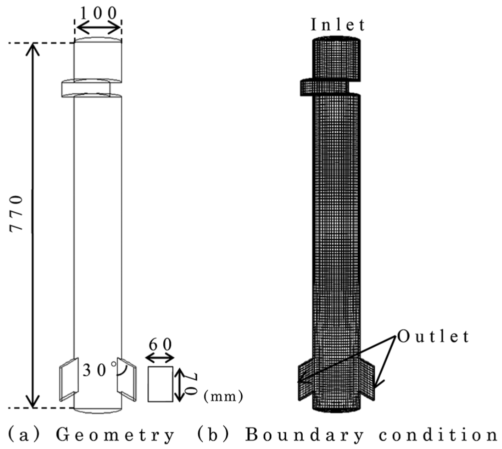

Fig. 2 Calculation geometry and mesh

Table 1 Calculation conditions

Molten steel	
Flow rate	2.4 ton/min
Density	7000 kg/m^3
Viscosity coefficient	0.006 Pa·s
Alumina particle	
Diameter	100 μm
Density	3990 kg/m^3
Concentration	40 ppm

mersion nozzle was set to 100 mm and the opening degree of the sliding gate was set to 75%. A uniform flow was assumed to enter the top of the immersion nozzle and the outlet port end was assumed to be under free outflow conditions. The height and width of the outlet ports were set to 70 and 60 mm, respectively. The angle of the outlet ports was set to 30° downward. Transient analysis was conducted under the conditions shown in **Table 1**.

2.2 Inclusion adhesion model

Figure 3 schematically illustrates the flow pattern near the nozzle refractory wall according to the description of the inclusion adhesion mechanism by Linder.[10] The inside diameter of immersion nozzles is generally 50 to 100 mm and the molten steel inflow rate is approximately 0.5 to 6.0 ton/min. The Reynolds number Re in the immersion nozzle is calculated to be Re = 1.06×10^5 by taking the inside diameter of 0.08 m as characteristic length and using the values given in Table 1. In a turbulent flow, the flow velocity decreases near the nozzle refractory wall under the influence of wall friction and a laminar flow region is formed. The laminar flow region is called a laminar sublayer or viscous sublayer. The thickness of the viscous sublayer δ is obtained from Equation (16).[18] In Equation (16), v is the kinematic viscosity coefficient of molten steel and u^* is the friction velocity of molten steel.

$$\delta = 5.0v/u^* \qquad (16)$$

The friction viscosity u^* is given by Equation (17). In Equation (17), τ_w is the wall friction stress and c_f is the average friction coefficient. From Equations (16) and (17), the thickness of the viscous sublayer is inversely proportional to the root square of the offshore flow velocity.

$$u^* = (\tau_w/\rho)^{1/2} = (c_f/2)^{1/2}u_{\mathrm{bulk}}^{1/2} \qquad (17)$$

Linder[10] assumed that the inclusion particles are introduced into the viscous sublayer by turbulent diffusion, they adhere to the nozzle refractory wall. The adhesion velocity V_T to the nozzle refractory wall is modeled as given by

$$V_T = 0.01d_P\frac{\tau_w}{\rho v} \qquad (18)$$

Similarly, Oeters[11] calculated the adhesion velocity to the nozzle refractory wall of intrusion particles introduced into the viscous sublayer by turbulent diffusion as given by

$$V_T = \frac{0.62\varepsilon^{3/4}\times10^{-2}}{v^{5/4}}\left(\frac{d_P}{2}\right)^2 \qquad (19)$$

Mukai et al.[19] reported the mechanism whereby inclusion particles enter the viscous sublayer and move to the nozzle refractory wall under the action of the surface tension gradient due to the concentration gradient near the nozzle refractory wall.

In this study, we considered the following four models as adhesion models of inclusions to the nozzle refractory wall:

1) Model in which the adhesion velocity is inversely proportional to the root square of the flow velocity
2) Model in which the adhesion velocity is inversely proportional to the root square of the flow velocity and is proportional to turbulent viscosity
3) Linder model
4) Oeters model

The first model (hereinafter referred to as model 1) is based on the premise that the lower the flow velocity, the thinner the viscous sublayer becomes and the more likely the inclusions adhere to the nozzle refractory. The second model (hereinafter referred to as model 2) is the model 1 to which is added such an effect that the higher the turbulent viscosity, the more readily the inclusion particles enter the viscous sublayer. The Linder model and Oeters model compare the test results and numerical analysis results of inclusion particles adhering to the nozzle refractory rotated in a crucible. The distribution of adhered inclusions calculated by the Linder model is reported to be close to the experimentally determined distribution of adhered inclusions.[20, 21]

A numerical analysis model can obtain the quantities required for the above four models to calculate the adhesion velocity of inclusion particles to the nozzle refractory wall. As a concrete calculation method, transient analysis is conducted on the time marching method and the adhesion velocity is calculated at each time step while the advection and diffusion of the inclusion concentration are being calculated. In the cells where the inclusions were adhered, the volume of the adhered inclusions was integrated. When the cells were filled up, they were defined as solid walls by using immersed boundaries. The clogging of flow channels was simulated in this way.

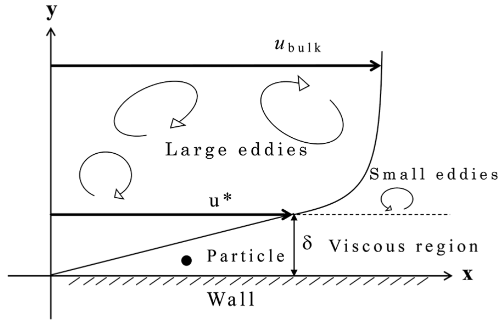

Fig. 3 Schematic illustration of flow situation close to wall

3. Numerical Analysis Results

Figure 4 shows the distribution of adhered inclusions and the distribution of molten steel flow velocity after 3600 s as the results of calculation by model 1. Model 1 assumes that the adhesion velocity of inclusion particles is proportional to the root square of the flow velocity in the cells adjacent to the nozzle refractory wall and to the inclusion concentration N. The calculations were made by setting the coefficient α of the adhesion velocity to 0.1.

$$V_T = \alpha N \frac{1}{\sqrt{v}} \tag{20}$$

Figure 5 shows the flow velocity distribution in an immersion nozzle of the initial geometry and the flow velocity distribution when inclusions are adhered to the immersion nozzle after 3600 s. When no inclusions are adhered to the immersion nozzle wall at t=0, the molten steel flows straight down through the opening of the sliding gate and stagnates in the open space of the sliding gate. The molten steel also stagnates downstream of the clogged region of the sliding gate.

With model 1, the adhesion of inclusions proceeds in low-flow velocity regions. At t=3600 s, as a result, large amounts of inclusions adhered in the open regions of the plate and the clogged regions of the gate. The amount of inclusions adhered near the outlet ports is relatively small. Inclusions are adhered in the concave portion (well) at the bottom end of the nozzle. This nozzle clogging is considered close to the nozzle clogging experienced on actual continuous casters.

Figure 6 shows the adhesion of inclusions when model 2 was applied. With model 1, the adhesion velocity depends only on the flow velocity and inclusion concentration, and the effect of the turbulence degree is not taken into account. Model 2 assumed that the adhesion velocity is proportional to turbulent viscosity in addition to the effects of flow velocity and inclusion concentration. The adhesion velocity is expressed by Equation (21). The coefficient α was adjusted to make the adhesion amount comparable to that in model 1.

Figure 7 shows the flow velocity distribution when the inclusions are adhered to the immersion nozzle. Model 2 considered the effect of turbulent viscosity but produced results similar to those of model 1 that did not consider the effect of turbulent viscosity. This is because the turbulence degree is high throughout the immersion nozzle and because there is no significant difference in the distribution of turbulent viscosity between models 1 and 2. This study used the k-ε model, the most standard turbulence model. It will be neces-

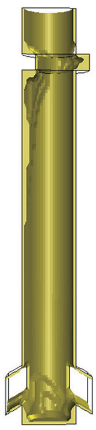

Fig. 4 Calculation result of nozzle clogged in model 1

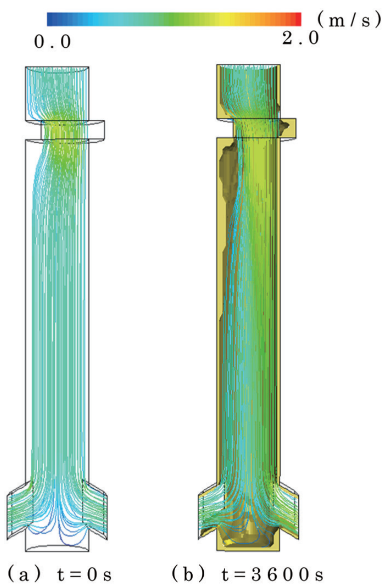

Fig. 5 Velocity distribution in immersion nozzle of model 1

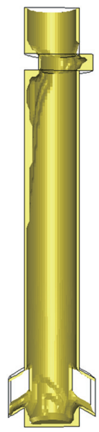

Fig. 6 Calculation result of nozzle clogged in model 2

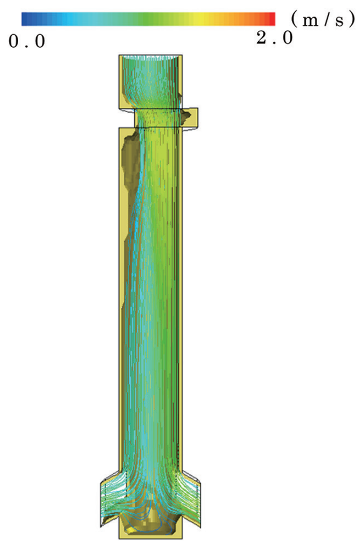

Fig. 7 Velocity distribution in immersion nozzle of model 2

sary to study the effect of turbulence models.

$$V_T = \alpha N \frac{\mu_t}{\sqrt{\nu}} \tag{21}$$

Next, the results of calculations with the Linder model and the Oeters model are shown in **Fig. 8**. **Figure 9** shows the flow velocity distributions with the adhesion of inclusions in the Linder model and the Oeters model. With the two models, the adhesion of inclusions proceeds where the turbulent energy dissipation rate is high and also proceeds around the outlet ports. The latter adhesion of inclusions could not be reproduced by models 1 and 2. The inclusions adhered in small amounts in the open regions at the center of the sliding gate. This is contrary to the conventional view that the inclusions adhere in large amounts in these regions.

Figure 10 compares the results of calculations with the nozzle clogging models studied. The horizontal sections of the upper, center and lower parts of the sliding gate and the enlarged views near the outlet ports are shown in Fig. 10. The adhesion amount of inclusions is large in the central open regions of the sliding nozzle in models 1 and 2, but small in the Linder model and the Oeters model. On the other hand, the adhesion of inclusions does not proceed near the outlet ports in models 1 and 2, but the outlet ports are clearly clogged in the Linder model and the Oeters model.

Nozzle clogging on the actual continuous caster is considered to proceed as shown in Fig. 1. The reproducibility of clogging around the sliding gate was better with models 1 and 2. The reproducibility of clogging around the outlet ports was better with the Linder model and the Oeters model.

4. Conclusions

Concerning nozzle clogging on continuous casters, we studied the adhesion of inclusions promoted by the molten steel flow velocity and obtained the following findings: We think that we can complete a model capable of evaluating nozzle clogging by comparatively studying the investigation results of nozzle clogging on con-

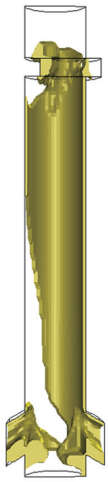

Fig. 8 Calculation result of nozzle clogged in Linder model and Oeters model

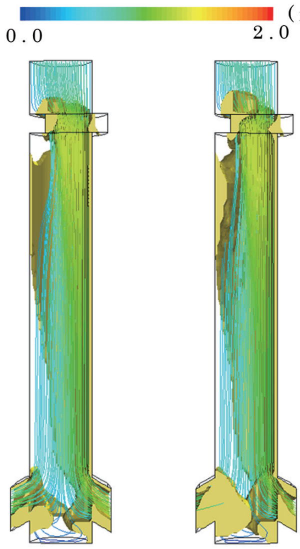

Fig. 9 Distribution of fluid flow in Linder model and Oeters model

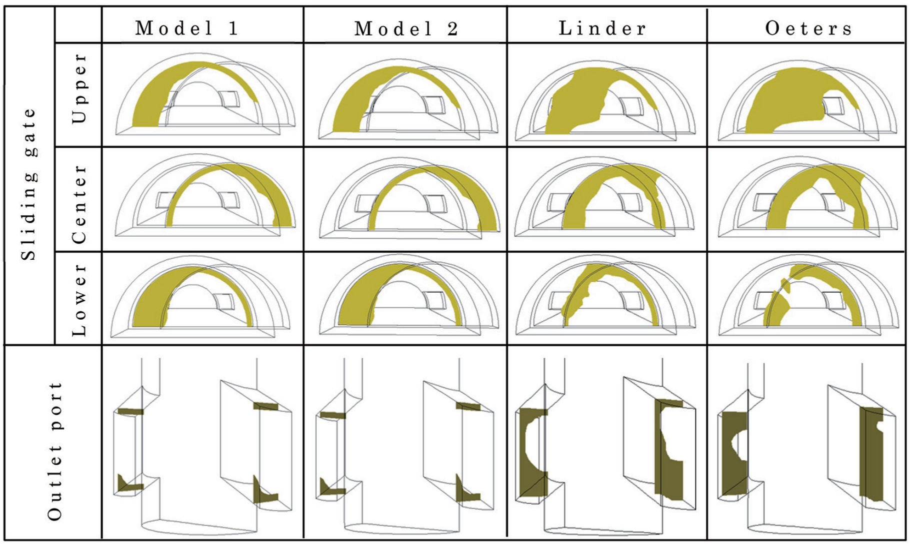

Fig. 10 Comparison of nozzle clogged in calculation models

tinuous casters and the numerical analysis results of nozzle clogging.

1) The adhesion of inclusions in the flow stagnant region around the sliding gate is satisfactorily reproduced by a model that assumes that the adhesion velocity of inclusions is inversely proportional to the square root of the molten steel flow velocity. However, this model cannot reproduce the clogging of the outlet ports.
2) The Linder model and the Oeters model can successfully reproduce the clogging of the outlet ports but assume that the amount of inclusions adhering in the open regions of the sliding gate is smaller than actually observed.

References

1) Kaneko, T., Ohno, T., Mizoguchi, S.: Tetsu-to-Hagané. 66, S868 (1980)
2) Fukuda, Y., Ueshima, Y., Mizoguchi, S.: ISIJ Int. 32, 164 (1998)
3) Ogibayashi, S., Uchimura, M., Maruki, Y., Mizukoshi, D., Tanizawa, K.: Proceedings of Steelmaking Conf. AIME, 1992, p. 337
4) Sasai, K., Mizukami, Y., Yamamura, H.: Tetsu-to-Hagané. 79, 1067 (1993)
5) Singh, S. N.: Metall. Trans. 5, 2165 (1974)
6) Taniguchi, S., Kikuchi, A.: Tetsu-to-Hagané. 78, 423 (1992)
7) Rubinow, S. I., Keller, J. B.: J. Fluid Mech. 11, 447 (1961)
8) Saffman, P. G.: J. Fluid Mech. 22, 385 (1965)
9) Mukai, K., Tsujino, R., Sawada, I., Zeze, M., Mizoguchi, S.: Tetsu-to-Hagané. 85, 307 (1999)
10) Linder, S.: Scand. J. Metall. 3, 137 (1974)
11) Oeters, F.: Metallurgy of Steelmaking. Düsseldorf, Verlag Stahleisen, 1994, p. 323
12) Thomas, B. G., Zhang, L.: ISIJ Int. 41, 164 (2001)
13) Kato, T., Hara, M., Muto, A., Hiraki, S., Kawamoto, M.: ISIJ Int. 47, 840 (2007)
14) Gutierrez, E., Garcia-Hernandez, S., Barreto, J. J.: ISIJ Int. 56, 1394 (2016)
15) Mizushina, T., Touei, R.: Introduction to Chemical Engineering (in Japanese). Tokyo, Sangyo Tosho Publishing, 2012, p. 230
16) Sambasivam, R.: Ironmaking Steelmaking. 33, 439 (2006)
17) Tsukaguchi, Y., Hayashi, H., Kurimoto, H., Yokaya, S., Marukawa, K., Tanaka, T.: Tetsu-to-Hagané. 95, 33 (2009)
18) Shirotuka, T., Hirata, A., Murakami, A.: Kenetics for Chemical Engineers (in Japanese). Tokyo, Ohmsha, 1966, p. 147–158
19) Mukai, K., Okuno, H., Tsujino, R., Ogata, K.: CAMP-ISIJ. 7, 213 (1997)
20) Okayama, A., Okada, N., Takatani, K.: CAMP-ISIJ. 25, 979 (2012)
21) Okada, N., Okayama, A., Takatani, K.: CAMP-ISIJ. 25, 980 (2012)

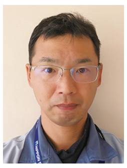

Nobuhiro OKADA
Senior Researcher, Dr.Eng.
Mathematical Science & Technology Research Lab.
Advanced Technology Research Laboratories
20-1 Shintomi, Futtsu City, Chiba Pref. 293-8511

Takehiko TOH
Dr.(Environmental Studies)
General Manager, Head of Div.
Resource and Process Solution Div.
Nippon Steel Technology Co., Ltd.

Hitoshi FUNAGANE
Researcher, Dr.Eng.
Mathematical Science & Technology Research Lab.
Advanced Technology Research Laboratories